Near Field X-ray Lithography to 15 nm.

Antony J. Bourdillon[0 a], Gwyn P Williams[b], Yuli Vladimirsky[a] and Chris B Boothroyd[c]
[a]UhrlMasc Inc., P.O. Box 700001, San Jose, CA 95170; [b]Jefferson National Accelerator Facility, 12000 Jefferson Avenue, Newport News, VA 23606; [c]IMRE, 3 Research Link, Singapore 117602

ABSTRACT

It is time to revisit X-ray. By enhancing, in the Near Field, Proximity X-ray Lithography (PXL), the technique is demonstrated that extends to 15 nm printed feature size with 2:1 ratio of pitch to line width. "Demagnification by bias" of clear mask features is positively used in Fresnel diffraction together with rapid, multiple exposures of sharp peaks. Pitch is kept small by multiple, stepped exposures of the intense image followed by single development. The optical field is kept compact at the mask. Since the mask-wafer gap scales as the square of the mask feature size, mask feature sizes and mask-wafer gaps are comparatively large. A Critical Condition has been identified which is typically used for the highest resolution. Many devices, including batches of microprocessors, have been demonstrated previously by traditional 1X PXL which is the most mature of the Next Generation Lithographies and which is now further extended. Throughput and cost are conventional.

Keywords: X-ray, PXL, Near field, Demagnification by Bias, Ultra High Resolution Lithography

1. INTRODUCTION

Given delays and difficulties in competing Next Generation Lithographies (NGLs), it is time now to revisit X-ray. Thisd has been on the Roadmap for Semiconductors since NGL issues were first addressed. X-ray is the only developed NGL[1], with many demonstrated devices including batches of microprocessors. X-ray is extensible, beyond other NGLs, to 15 nm[23]. It is ready to go at 45 nm. Its cost and throughput are, uniquely for NGLs, conventional. X-ray uses proximity printing in a simple experimental arrangement.

It is well known that in December of 1998, the semiconductor industry in the United States voted X-ray third for implementation behind extended ultraviolet lithography (EUVL) and scattering limited projection electron beam lithography (SCALPEL). The last two are projection techniques that use narrow band without the planar collimation provided naturally in relativistic light sources. The projection methods have suffered low throughput and in the former case additional very high cost. They are physically more complex than proximity printing.

Key issues for NGL are cost, throughput and yield. Added to these is, now, demonstration [1]. There has been a general failure to recognize the development that has occurred in X-ray, both incremental and with breakthrough advances. For example, using demagnification by bias, prints with feature size down to 25 nm have been demonstrated [2,3,4,5,6,7]**.** With the 'demagnification', dense lines have been demonstrated [2]. Neither lenses nor mirrors are used between mask and wafer. Typical 1-2kV broad band incident beam energies (1.2-0.6 nm wavelengths) were used, and demagnifications down to 6X were obtained. The mask feature sizes and mask-wafer gaps were large, about 20 µm. The technique, which has many novel features and is sometimes called Ultra-High Resolution Lithography[8] (UHRL), employs Fresnel diffraction positively near a "Critical Condition" (see below and ref. [2]) and results in the demagnification by bias. While the print is smaller than the corresponding clear mask feature, the demagnification is not generally uniform because the bias is more or less constant around the edge of the image so that the bias is subtracted from the size of the mask aperture when the print is developed. Meanwhile, the optical field is kept compact as in traditional 1X PXL, and printed lines are kept dense by multiple exposures of sharp peaks in Fresnel imaging. The demagnification has

1 [0]bourdillona@prodigy.net; phone/fax 408 777 0577; www.UHRL.net

considerable importance in a wide range of applications including integrated circuit manufacture[9] and manufacture of micro electromechanical systems. The importance is due additionally to the relative physical simplicity of proximity methods over competing projection systems, as also to relatively high throughputs and simple equipment requirements.

Thus PXL, which is the only one of the next generation lithographies [1,10,11,12,13,14] that is properly demonstrated, is extensible beyond previously supposed limits. Typically, synchrotron radiation is used as the radiation source and this is naturally collimated by relativity so that the penumbra is controlled to within one nanometer. To provide uniform illumination, the X-ray beam is typically scanned, off an oscillating, grazing-incidence mirror, across the mask-wafer system. Exposures of full fields, typically 50 x 30 mm, are made in a time about 1 s. The mask is held stationary while the wafer is stepped and aligned between exposures on different fields.

Previously, we have reported the results of simulations [2,15] that have shown the effects of (a) varying the mask-wafer gap about the critical condition; of (b) the residual effects of small absorber transmission, of (c) the distortion to be observed in non-symmetric, two-dimensional features, of (d) high frequency "ripple" and "bright spots" parallel to longer dimensions, of (e) mask shaping to virtually eliminate the "ripple" and "bright spots", and of (f) combined doses due to multiple exposures used to reduce pitch:line width [2]. The simulations have been performed for both monochromatic incident radiation and for the wide band of wavelengths typically used in PXL. The simulations generally correspond to earlier experimental demonstrations [2,3,4,5]. Here, after outlining the quantal advance gained by Near Field X-ray, we show how development levels are optimized in the printing of features having complex shapes, and we discuss a variety of methods for making magnification corrections when using either synchrotron sources or the slower X-ray point sources.

We have previously listed other attempts at fine printing by methods equivalent to 1X contact printing [5]. There have been further incremental attempts to enhance PXL some of which can, in principle, be employed in Near Field to extend further to 15 nm printed features. Some attempts have been uncompetitive for high resolution[16] and involve unnecessarily complicated procedures in 1X mask making and exposure for phase shifting. More significant is the attempt to use shorter wavelength X-rays, about 0.4 nm, with diamond-like mask substrates [17,18] and modified resists. It is clear that such incremental resolution enhancements can be improved by a large factor of 3 when adapted to Near Field. This is partly due to the larger mask-wafer gaps that can be employed, since the gap scales as the square of the clear mask feature.

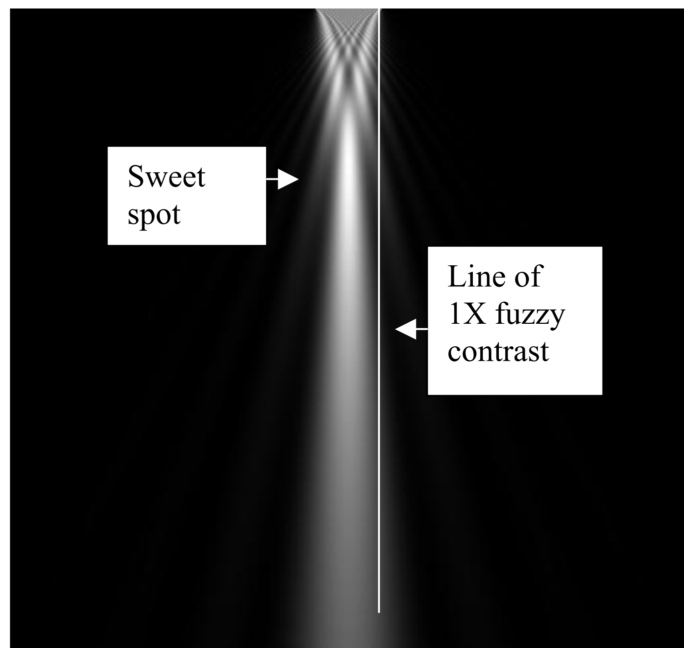

Fig 1. Universal current or flux distribution from clear mask feature simulated in Fresnel diffraction.

2. SWEET SPOT

2.1 Currents from a clear mask feature

To illustrate graphically the necessity for demagnifying clear mask features, when high resolution is needed in PXL, we simulated currents transmitted. Further details showing the effects of residual absorber transmission are given elsewhere [2] and are supplemented by the analysis of temporal coherence described below.

Fig. 1 is a universal dimensionless image showing the distribution of current below a clear mask feature. If the clear mask feature has a width of 150 nm and the wavelength is 0.8 nm, then the vertical range shown is about 40 µm. With 0.4 nm wavelength, the range is 80 µm. It can be seen that there is a long "sweet spot" about one quarter down where the current is bright and narrow. The 'depth of focus' is several microns. The sweet spot corresponds to the Critical Condition (CC, see below). Here, by controlled development, the highest resolution can be obtained since the single peak in the aerial image is most narrow. Further theoretical description of this optimum is given below.

The line of fuzzy contrast shows the low development level used in all previous demonstrations of traditional 1X proximity printing, some of which are listed in table I[19]. In Near Field X-ray, the sweet spot is used to extend the print resolution.

Table I. Some devices demonstrated using X-ray

- 1Gb DRAM test site, excellent bit yield in 1 Mb arrays (IBM VLSI '98)
- 1Gb DRAM test site (Ru/BST/Ru stacked>25fF/cell capacitor with 0.14 µm gates (Mitsubishi, IEDM '95)
- 4Gb DRAM test site, functional cells with 0.24 µm pitch 4 levels X-ray (Toshiba/NTT, IEDM '96)
- 64 Mb DRAMS 63.98 functional bits (IBM SPIE '95)
- 400 MHz power PC 604 e, 0.24 µm gates, batches (IBM Photomask, Jn '99)
- 0.375 CMOS logic, fully functional 1 Mb SRAM, 3 levels X-ray (Motorola, DARPA '96)
- 0.2 µm switching control units fully functional, 6.4M transistors (NTT EIPN '96)
- 0.1 µm CMOS devices functional ring oscillators with stage delays of 16 ps (IBM EIPN '95)
- 0.2 µm LSI communications circuits, fully functional 8x48 bit multiplier, 12 kb SRAMS (NTT/EIPBN '96)
- 0.2 µm CMOS logic, fully functional 64 kb SRAMS (IBM, IEDM '94)

Schematic for demagnification by bias with multiple exposures for nested features.

The peak at the sweet spot is illustrated in the schematic fig. 2 where the sharp peak at CC allows rapid exposure above a broad background. The ratio of pitch to line-width is reduced to 2:1, i.e. half pitch, by the method of multiple exposures with single development. The process is rapid because the peaks are intense and the stepping is typically blind. The schematic shows how nested features have been printed[2,3].

3. DEMONSTRATIONS

The following demonstrations were performed on a modified Suss XRS-200/2M X-ray stepper, owned by the Center for Nanotechnology and located on beamline ES-4 on the Alladin storage ring at the University of Wisconsin-Madison Synchrotron Radiation Center. A combination of optimized lithographic process and exposure conditions allowed the formation of lines down to 25 nm at 15-30 µm gaps for both negative (SAL605) and positive (UV-3, APEX-E) resists [20]
.

3.1 Line prints using demagnification by bias

To demonstrate the fact of demagnification by bias, various line prints have been recorded using a synchrotron radiation source with a typical broad band radiation dose centered about 0.8 nm wavelength [2, 3]. An example is shown in fig. 3. SAL 605 resist was used in fig. 3a and PMMA in fig. 3b. Further examples are shown in reference 2 and elsewhere. The references also show demonstrations of nested lines made with a double exposure

.

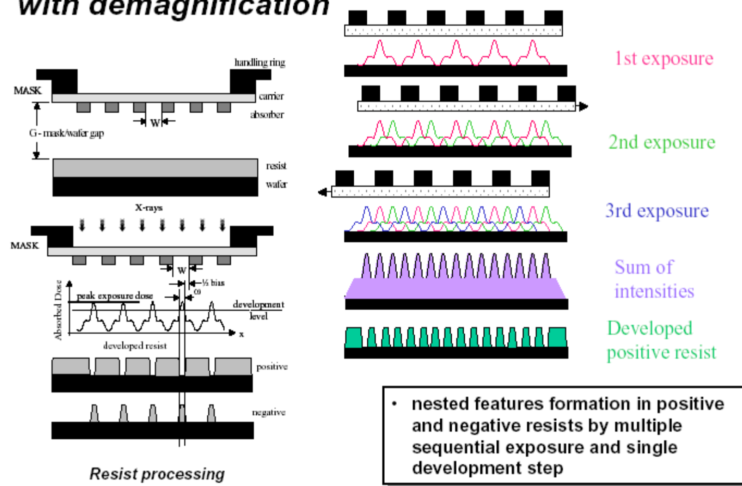

Fig. 2. Schematic diagram shows dense lines developed from multiple exposures of individually demagnified clear mask features 3 (courtesy Institute of Physics Publishing [2])

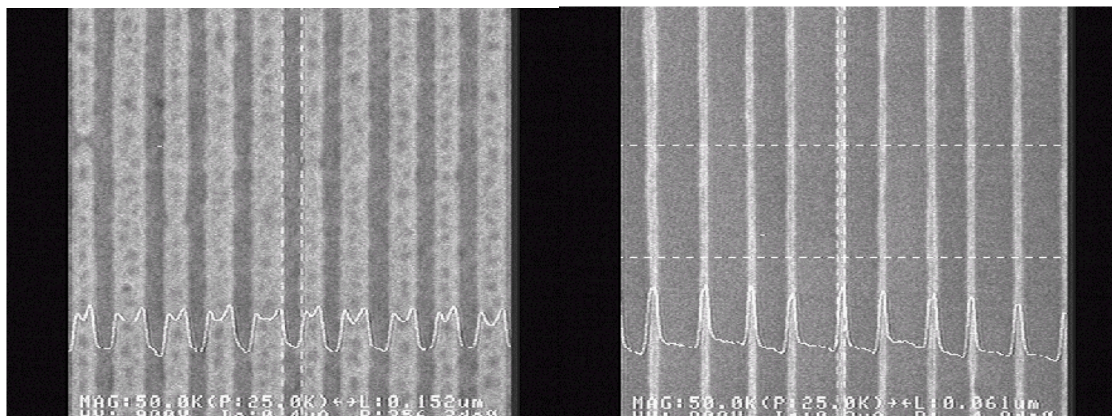

Fig. 3a. 61 nm lines printed in SAL 605 negative resist using a mask with 180 nm nominal line/space features (360 nm period). Left mask (152 nm); right print (61nm). Courtesy Institute of Physics Publishing [2].

4. TEMPORAL AND SPATIAL COHERENCE

4.1 The Critical Condition in one dimension

Consider firstly the Critical Condition as it applies in the imaging and printing of one dimensional features such as parallel lines. Fig. 5 shows a schematic exposure system. Parallel rays of radiation pass through a clear mask feature and form a Fresnel pattern, or demagnified image, at a distance G below the mask feature. One ray is axial. A second ray suffers a phase lag which depends on the distance, s, from the center line of the clear mask feature, i.e. the phase lag suffered by this ray at the resist depends on $2\pi s^2/\lambda$, when the wavelength is λ. The amplitude at the wafer depends on the vectorial sum of the amplitudes of all rays passing through the clear mask feature.

Consider the dimensionless spatial coordinate, ν , defined:

$$v = s\sqrt{\frac{2}{G\lambda}} = \sqrt{2\tilde{N}_F} \quad , \qquad (1)$$

where s is a distance measured from the axis of the clear mask feature/clear mask feature in its plane (fig. 5); G is the width of the mask/wafer gap; λ is the wavelength of the radiation used, and N_F is the number of Fresnel half zones across the clear mask feature.

If Δ*s* is the clear mask feature width and Δν is the dimensionless spatial co-ordinate corresponding to Δ*s* at a given *G* and λ then:

$$\Delta v = \Delta s\sqrt{\frac{2}{G\lambda}} \quad , \qquad (2)$$

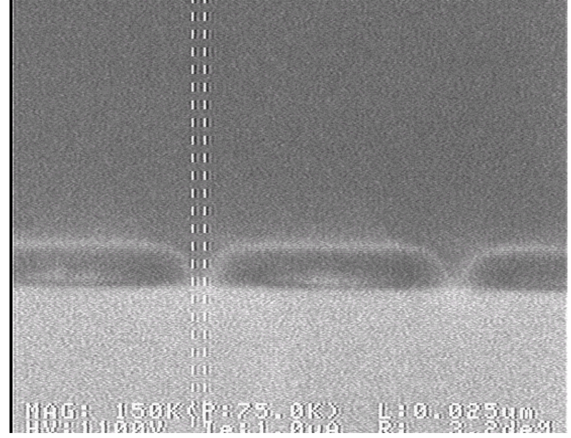

Fig. 3b. 28 nm and 25 nm prints in positive resist

Δν can be called the dimensionless slit width. The vectorial addition of the amplitudes and phases of rays passing through the clear mask feature, and interfering constructively at the plane of the wafer, can be summed over all transmitted rays. The amplitudes are represented mathematically with well-known Fresnel integrals or can be summed graphically with Cornu's spiral[21], i.e. the vibration curve, shown in fig. 5. The amplitude of the Fresnel pattern at a point on the wafer can be found by summing amplitudes and phases of corresponding rays [12]. The vectorial summation is found graphically by connecting two points on Cornu's spiral. The *Critical Condition* occurs when the width of a transmitting mask feature, Δ*s*, is related to the mask/wafer gap G and X-ray wavelength λ by the equation:

$$\frac{\Delta s}{\sqrt{\lambda G}} = 1.7 \qquad (3)$$

At the Critical Condition, summing over rays for which Δs/2 > s > -Δs/2, the amplitude at the wafer, on axis, is the longest vector which joins the extremities of the Cornu spiral. This vector is represented by the Critical Vector **C** in fig. 5. The square on this vector is the maximum intensity. Off-axis at the wafer, asymmetric vectors on the spiral are used to represent vectorial sums of ray amplitudes.

The Critical Condition has a clear theoretical meaning with practical implications. However there is wide latitude in setting the conditions - through the selection of wavelength, mask feature size and gap - which are not practically critical. Cornu's spiral applies to the imaging of a long slit with monochromatic radiation; but we extend it, as described below, to applications using broad band illumination having temporal incoherence.

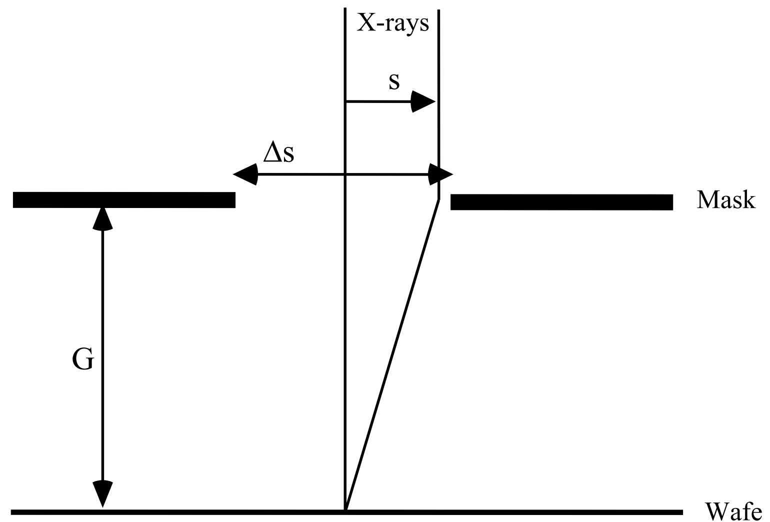

Fig. 4. Rays that are transmitted off-axis suffer phase shifts equal to $2\pi s^2/\lambda$. These shifts are represented on the Cornu spiral in fig. 5.

Notice meanwhile that, by holding the dimensionless spatial coordinate $\Delta\nu$ in equation 2 constant, the gap, G, changes with the square of the slit width,Δs, and that G depends inversely on λ. This is an important reason for demagnifying and a new reason for using shorter wavelengths [15] .

4.2 The Critical Condition with Broad Band Illumination

Secondly, with broad band illumination, simulations require independent integration for both temporal and spatial coherence. When the wavelength, λ , is not monochromatic but is spread over a range $\delta\lambda$, it follows from equation 1 that $\delta\nu/\nu=-\delta\lambda/2\lambda$. The Fresnel integrals, represented in Cornu's spiral, can be averaged as in the greyscale curves in Fig 5. The averaging procedure, by including vectorial additions of rays, accounts for the temporal coherence. Specifically, with broad band illumination, such that the bandwidth corresponds to $\delta\nu = \pm 0.2$, the ray phases can be represented by the tangents on the corresponding curve in fig. 5. Corresponding phases at a wafer, for bandwidth ranges $\delta\nu = \pm 0.4$, and, for bandwidth ranges $\delta\nu = \pm 0.6$, are represented on corresponding curves. Summing rays over the dimensionless slit width provides corresponding aerial profiles. A few examples are given in fig 6.

The new significance of these plots lies in the inflection points where the graphs at various $\delta\nu$ cross over. The inflection points closest to the axis (ν=0) occur at $\nu = \pm 0.36$ where the slope is steeper, and at $\nu = \pm 0.88$ where the slope is shallower. A steep slope is valuable for critical dimension (CD) control in printing. It is interesting, furthermore, that the inflection points occur on the same ordinate scale as the incident intensity (level 2) at the clear mask feature.

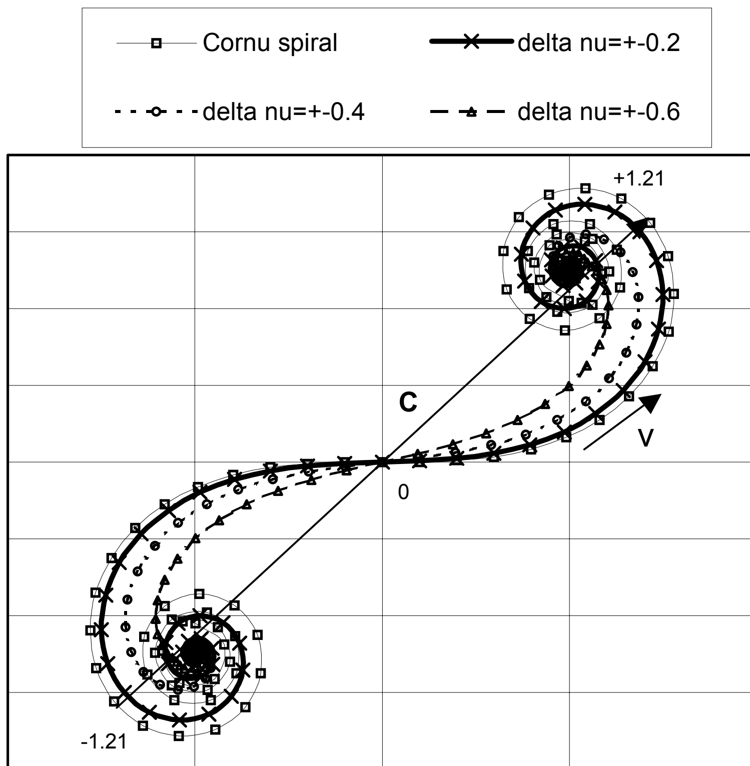

Fig. 5. Cornu's spiral [1], (full line) representing relative phases of rays transmitted by a slit onto a wafer. Vector A represents the sum of phases of monochromatic, transmitted rays, striking the wafer at the Critical Condition, opposite the slit axis. Other spirals are formed by averaging over spreads of dimensionless spatial co-ordinates: typically when $\delta\nu = \pm 0.2$ (dashed curve), and also when $\delta\nu = +0.4$ (dotted curve) and $\delta\nu = +0.6$ (dash-dot curve). These spreads correspond to broad band illumination and are used to show the effect of temporal incoherence.

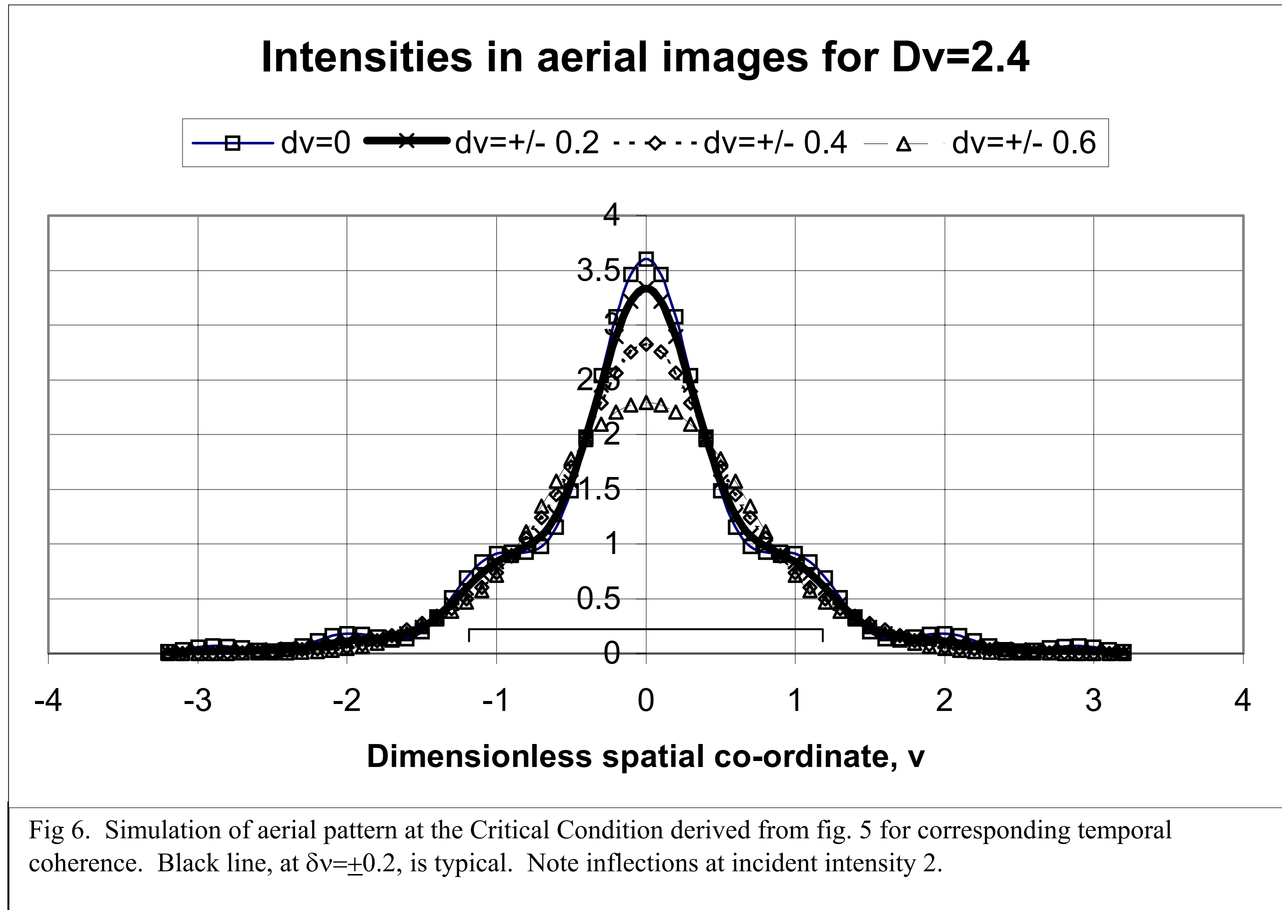

Fig 6. Simulation of aerial pattern at the Critical Condition derived from fig. 5 for corresponding temporal coherence. Black line, at $\delta\nu=\pm0.2$, is typical. Note inflections at incident intensity 2.

When $\nu = 0.88$, and $\delta\nu = 0$, the printing definition is extremely poor. This is close to the case used in traditional 1X proximity printing 8 where $\nu = 1.2 = \Delta\nu/2$ at the Critical Condition. Contrast is then further degraded with broad band as can be seen in fig. 6 and additionally degraded by sidebands. Compared with the aerial image shown in the fig 6, sidebands at $\nu > \Delta\nu/2$, are increased by residual transmission from the mask absorber [4] and further increased in masks containing periodic structures. The fuzzy contrast, sometimes difficult to predict, that was traditionally used in 1X PXL is completely avoided in Near Field where rapid exposures are made, high on the aerial image instead of at the base.

However, the inflection points demonstrate a further optimisation of demagnification in Near Field. Previously, we have proposed [5] that demagnification by bias is selectable, depending on chosen development level and that optimisation depends on various factors including fabricability of masks and multiple exposure systems. It now appears that an additional feature needs to be taken into account and this may often dominate: where CD control is critical, contrast is highest at the inflection point, i.e. at a demagnification of 3X or 1/0.36. The inflection points occur at the dose level of incident radiation at the mask

4.3 The Critical Condition for Two Dimensional Features

Consider thirdly the critical condition for two dimensional, asymmetric, clear mask features. Since the CC depends on clear mask feature size, Δs, it cannot be maintained for two different dimensions at one time. CC then refers, by our convention [15] , to the smaller dimension where the print resolution is the more critical.

Consider in consequence, features produced in the less critical, longitudinal direction of a rectangular mask. To understand the independent effects of mask feature shape, wavelength and gap for the 2D images, idealized aerial

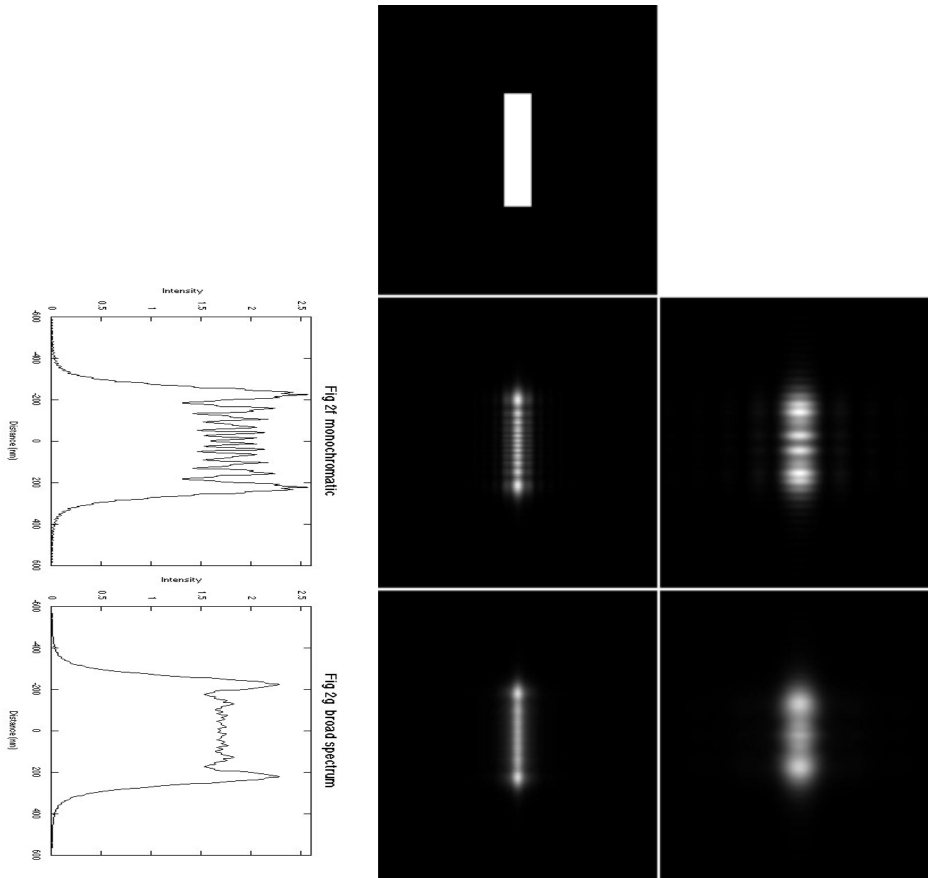

Fig.7a At top is a two-dimensional rectangular mask slit of size 150 x 600 nm^2 with intensity scale white=1; at centre a simulated image due to 0.8 nm X-rays transmitted at a distance 9.8 μm through the clear mask feature behind the otherwise opaque mask, i.e. for critical $\Delta\nu = 2.4$ and intensity scale white =2.7; at center bottom corresponding simulation with broadband $0.62<\lambda<1.28$ nm; at right corresponding simulations at distance 30 μm behind the opaque mask when $\Delta\nu=1.4$; at left corresponding central profiles of adjacent images. Notice that the "Ripple" and "Bright Spots" most evident in the central image, are reduced with broadbeam. (Courtesy Institute of Physics Publishing [17])

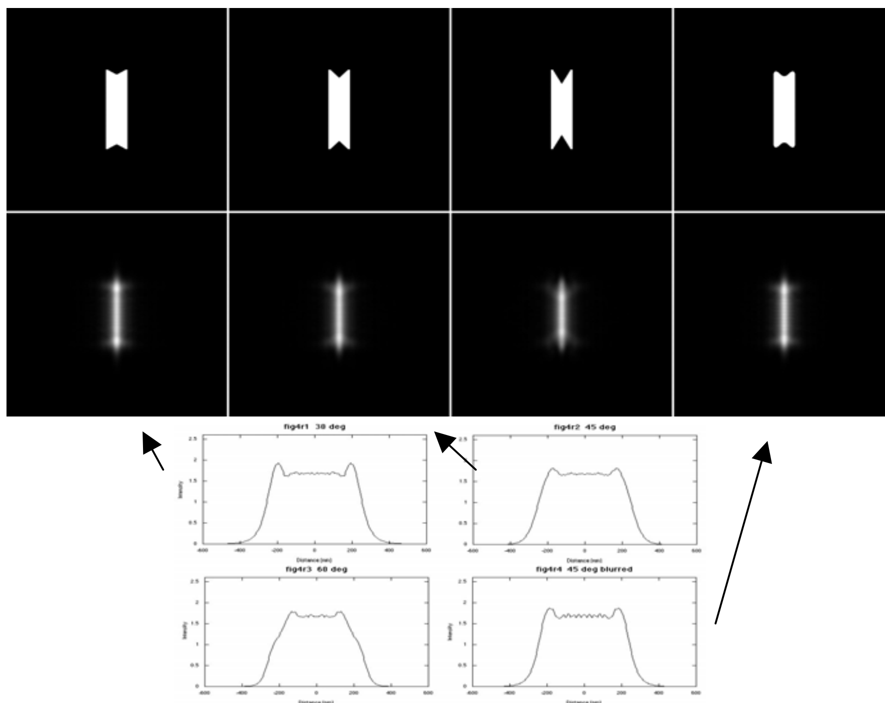

Fig. 7b Simulation of two dimensional rectangular mask as in fig. 7a but with indents: V-shaped 30^0; 45^0; 60^0 and blurred 45^0 and corresponding simulated images at the Critical Condition with broadband. Profiles are also shown. (Courtesy Institute of Physics [17])

patterns were simulated. The SEMPER program allows Fresnel diffraction from arbitrarily shaped masks in one or two dimensions to be calculated at any distance from the mask. Examples of imaging with monochromatic radiation and with broad band illumination, both at CC and away from CC, are shown in fig. 7a [1,11]. This shows the leveling of both "Ripple" and "Bright spots" in the pattern when broad beam is used. The leveling is a consequence of temporal incoherence.

To reduce undesirable effects of Ripple and Bright spots further,

the spatial incoherence in the aerial pattern can be increased by an inverted variant of optical proximity correction. An example is shown in fig. 7b The blurred 45 degree indent, at the ends of the rectangular pattern, results in a reduction of Ripple and Bright spots to insignificance when broad beam is additionally used, typically, as before.

Elsewhere [2,4], the application of temporal and spatial coherence to the printing of complex shapes has been described. In particular, a simulation of a flag pattern shows how intensity variations can be controlled. To print complex shapes with single exposures and optimum resolution, it is necessary to minimize Ripple and Bright Spots which otherwise limit development levels.
Simulations were performed for the intensities generated below the mask. A multislice method written in the SEMPER [22] image processing program was used.

Fig. 8 shows a simulated image of a bridge corresponding to the mask in the upper figure. As explained below, this simulation is actually due to a double exposure with an intermediate shift of 20 nm to minimize Ripple. If the bridge is 100 nm wide in the mask, a print 30 nm wide will be readily obtained using wavelengths $1.2>\lambda>0.6$ nm. In single exposures, an unfortunate horizontal Ripple occurs at the bridge contact[2]. We have previously shown how the Ripple can be reduced by wavy edges on the mask; but with an introduction of artifacts [4]. A combination of ten X-ray wavelengths with $0.62\leq \lambda \leq 1.24$ nm were used to simulate a synchrotron spectrum for a mask-wafer Gap of 4.3 μm , as is Critical for a 100 nm wide bridge at the mask.

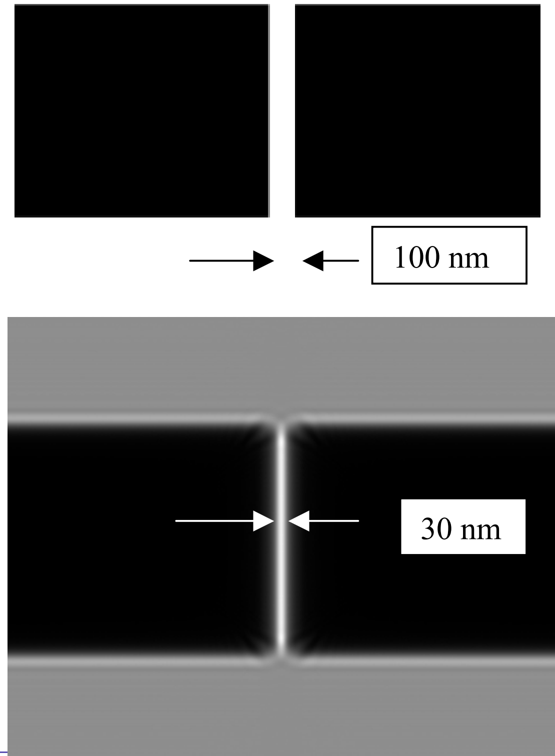

Fig. 8. Mask for bridge (top) 100 nm wide and image simulation made using SEMPER as before with wavelength $0.6<\lambda<1.2$ nm, but with mask-wafer gap G=4.3 μm. In this image Ripple is controlled by a double exposure with 20 nm shift. A typical print will be 3X for 30 nm at the bridge and just less than 1X at the contacts.

Now we show how, when the mask in fig. 8 is shifted between double exposures, the principal peak and trough on the horizontal contact ripple can be smeared. The Ripple can be controlled by optimization [2] of the shift to reduce both principal and subsidiary ripples. A remnant of the principal peak can be seen in fig. 8, but the troughs have been greatly reduced to allow raising the development level. This has many advantages including higher resolution, reduced exposure time and flexibility in making single exposures of complex patterns. The method of double exposures, used to reduce ripple at the contacts, provides a further degree of freedom in further reducing the ripple in two dimensional structures.

4.4 Extensibility to 15 nm and further

Various facts have led us to revise our previous estimates of the extensibility of Near Field methods [2, 4]. Though primary photoelectric blurring is broad, the printed contrast, in fact, depends on the Auger electrons, and their range is not only considerably smaller than that of the primaries, but moreover does not change with increasing incident photon energy. This range only changes significantly with resist composition which can be selected for optimization.

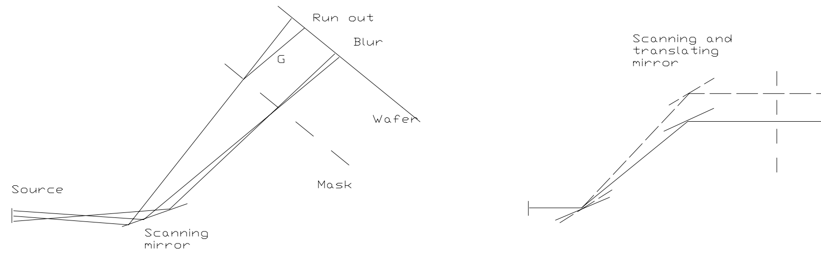

Fig. 9. Schematic diagrams showing (left) occurrence of blur and of Run-out or "magnification error," and (right) showing magnification correction by a scanning and translating mirror with X-ray beam incident horizontally at the mask. Not shown, for simplicity, is the conventional horizontally collimating mirror close to the tangent point that can be controlled to produce magnification corrections in the horizontal plane.

Blurring due to the range of Auger electrons is small down to configurations designed for 15 nm prints with Near Field. The diffraction limits depend on the experimental *k* value (k = smallest print feature size / $(\lambda\ G)^{1/2}$ ~0.15) demonstrated using demagnification by bias on isolated lines [6]. At dimensions for 15 nm prints, the gap approaches an experimental limit about 5 μm, and the printing is facilitated if a restriction to half pitch is relaxed.

4.5 Blur and Run-out in Proximity X-ray Lithography

Consider next, features in PXL that vary with the different sources that are sometimes used: the synchrotron source; the laser plasma point source that can be used without collimation [23] or with collimation [24,25], and the pinched plasma source employing electric discharge [26].

All of these sources use a broad band spectrum of wavelengths, up to 50% of mean wavelength, and share this advantage over projection methods which are by comparison complex, slow and costly. The synchrotron is especially intense because of the collimation provided by relativistic flattening of space onto the orbit plane and this is reflected in table I. The table also shows comparatively, the particular source properties of local and global divergence. These properties determine blur and "Run-out" (fig. 9 and table I).

On a synchrotron, penumbral blur depends on its effective source size, *z,* namely the electron beam cross-section as projected by the orbital motion. In practice the projection hardly increases the effective beam size, and a typical blur, *B*, in lithography systems having beam line length, *x*, from tangent point to mask, is given by $B=zG/x \sim 1$ nm 27 . The "Run-out" ΔM, or "magnification error," depends on the mask width, *w*, and gap: $\Delta M=wG/2x$.

If not corrected, Run-out causes a magnification error in 1X proximity X-ray lithography. Happily, several methods are available for making the correction. In one of these, a mirror is inserted between the first scanning mirror and the mask (fig. 9). The mirror is controlled to scan and translate in accord with the first scanning mirror [28], Run-out is virtually eliminated in the vertical plane. Likewise the run-out can be corrected in the horizontal plane by the horizontally collimating mirror normally placed close to the synchrotron tangent point in order to optimize collection. By an extension of the technique [29] with various controls, magnification corrections for the mask or wafer can also be made both horizontally and vertically. These optical methods are in addition to several other methods that have been proposed: the mask can be strained mechanically in vertical and horizontal planes [30]; or dynamic scanning of mask and wafer can produce vertical corrections [31]. On the synchrotron, blur and Run out are most readily controlled and adapted to overlay requirements in multiple level printing of integrated circuits.

5. CONCLUSION

Near Field X-ray Lithography is an enhancement of a well demonstrated technique that is extensible to 15 nm and that is conventional in both throughput and cost. There has been considerable interest[2324] in extending demonstrations to the 15 nm regions. Near Field X-ray Lithography has many advantages including control of printing, increased wafer throughput, increased mask feature size and gap width, in addition to the outstanding feature of extensibility beyond 20 nm. The method opens the way to the manufacture of micromachines and integrated circuits of such small dimensions, whether using modern compact synchrotron light sources[25] or, at a slower rate, with point sources[26].

Table I

Comparison of power, thoughput and divergence of various sources

	Emission W/sr	**Capture angle/msr**	**Exposed area/mm**	**Intensity delivered /mWcm**-2**	**Exposure time/s [a]**	**Throughput compared /8"wph**	**Local divergence /mrad**	**Penumbral blur/nm**	**Global divergence /mrad**	**Run-out (max) /nm**
Helios II	60,000 ~orbit plane	0.015	50 x 30 scanned	100	0.6	120 [b]	0.1	1	1.5 vertical 2.5 hor.	15 25
with collimation	60,000	0.015	50 x 30	100	0.6	120 [b]	~0.1	~1	< 0.25 [c]	2 [c]
Laser	3.8	0.9	50 x 50	~0.2	300	1	0.1	1	25	250
with collimator	3.8	35	22 x 22	~0.8	75	1.4	4	40	< 0.5	< 5
Squeezed Plasma	~4	0.9	50 x 50	~0.2	300	1	1	10	25	250

A Assuming chemically amplified resist with dose sensitivity 60 mJ/cm**2

B Allowing 0.4s alignment

C mask magnification error also correctible

.

REFERENCES

1. Gomba G A, Oral presentation at *Microlithography 2003*, paper 5037-01 Santa Clara, February 23-28, 2003. This was the keynote in the Emerging Lithographic Technologies session.
2. Bourdillon A J , Boothroyd C B , Williams GP and Vladimirsky Y, *J.Phys.D: Appl.Phys*. **36** (2003) 2471-2482
3. Bourdillon A J , , Williams G P, Vladimirsky Y and Boothroyd C B, *Microlithography 2003, SPIE* vol. 5037, pp 622-633
4. Bourdillon A J , Boothroyd C B , Kong J R and Vladimirsky Y, *J.Phys.D: Appl.Phys*. **33** (2000) 1-9
5. Vladimirsky Y, Bourdillon A J , Vladimirsky O , Jiang W and Leonard Q, *J.Phys.D: Appl. Phys.* **32** (1999) L114-L118
6. Kong J R, Vladimirsky Y and Quinn L, *Proc. MNE 2000*, Jena Sep 18-21, Germany
7.Kong J R, and Quinn L,Vladimirsky Y and Bourdillon A (2000), *Proc SPIE Microlithography 2000*, Santa Clara 27 Feb-3 March
8.Y Vladimirsky and AJ Bourdillon, *US patent Nr. 6,383,698* (2002)
9. *Solid State Technology*, February 2000, News Item, pp18-23
10. Neureuther A R, "Microlithography with soft X-rays" in *Synchrotron Radiation Research*, ed. Winich H and Doniach S, Plenum
11. Vladimirsky Y **"**Lithography**"**, Ch.10, in *Vacuum Ultraviolet Spectroscopy II,* pp.205-223; Eds. J.A.Samson and D.L.Ederer, (*Experimental Methods in the Physical Sciences*, Vol. **32**, Academic Press, 1998)
12. Cerrina F, "X-Ray Lithography", Ch. 3 in *Handbook of Microlithography, Micromachining, and Microfabrication,* Vol.**1**, ed. P.Rai-Choudhury, pp. 253-319 (SPIE Press, Bellingham, Washington, USA, 1997)
13. Krasnoperova A A, Rippstein R, Flamholz A, Kratchmer E, Wind S, Brooks C and Lercel M, *Proc SPIE conf.* vol. 3676, pp. 24-39 (1999)
14. Vladimirsky Y, "Introduction: limits or limitations" in *Proc SPIE conf.* Vol 3676, pp. xvi-xvii (1999)
15. Bourdillon A J and Boothroyd C B *(2001) J.Phys.D: Appl. Phys.* 2001 **34** 3209-3213
16. Yang L, Taylor JW, *J Vac Sci & Technol B* **19** 129-135 (2001)
17. Khan M, Han G, Bollepalli SB, Cerrina F and Maldonado J, *J Vac Sci & Technol B* **17** 3426-3432 (2000)
18. Khan M, Han G, Tsvid G, Kitayama T, Maldonando J and Cerrina F, *J Vac Sci & Technol B* **19** 2423-2427 (2002)
19. Proceedings, NGL Workshop, December 9, 1998. The data were presented again by Gomba in ref. 1.
20. Vladimirsky O, Dandekar N, Jiang W, Leonard Q, Simon K BollepalliS, Valdimirsky Y and Taylor JW (1999), *Proc SPIE Conf. vol 376 92*
21. Jenkins FA and White HE, *Fundamentals of Optics,*4th ed. McGraw-Hill 1976
22. Saxton W O, Pitt T J and Horner M (1979) *Ultramicroscopy,* **4**, 343
23. www.jlab.org/FEL/xrl_report_1.pdf
24. www.jlab.org/~gwyn/xrl_report_2.pdf
25. H.I.Smith, *Japan could dominate industry with X-ray Lithography*, Semiconductor International Vol 24, No. 2 pp 67-72 (2001).
26. Turcu I C E, Gaeta C J, Forber R A, Rieger H, Cassidy K L, Campeau S M, Hark P, Maldonado J R, Morris J H Carosella J H, Smith H, Lim M, Chen Z, Burdett J, Gibson D M, Whitlock R R and Dozier C M*, Proc SPIE Microlithography 2003*, vol 5037, Feb 23-27, to be published.